Novel Manta Rays Foraging Optimization Algorithm Based Optimal Control for Grid-Connected PV Energy System

FAHD A. ALTURKI[1], HAMMED O. OMOTOSO [1], ABDULLRAHMAN A. AL-SHAMMA'A [1,2], HASSAN M. H. FARH [1], AND KHALIL ALSHARABI [1]

[1]Electrical Engineering Department, College of Engineering, King Saud University, Riyadh 11421, Saudi Arabia
[2]Department of Mechatronics Engineering, College of Engineering, Taiz University, Taiz 6803, Yemen

Corresponding author: Abdullrahman A. Al-Shamma'a (ashammaa@ksu.edu.sa)

ABSTRACT Large-scale photovoltaic system (PV) installation can affect power system operation, stability, and reliability because of the non-linear characteristic of the PV system installation. DC/AC and DC/DC converters are the major devices use in connecting PV into the grid. These converters are liable to power quality problem if the proper control mechanism is not adopted. This study presents an optimal control technique to improve dynamic operation of PV grid-connected system. An optimal control method with use of Manta ray foraging optimization (MRFO), is implemented as a control strategy for tuning the proportional–integral (PI) controllers of DC/DC and DC/AC converters for the integration of the PV system into the grid. The MRFO is chosen because of its ease of implementation and requirement of less adjusting parameters. The effectiveness of the proposed technique is studied under irradiance variation. The obtained results demonstrate the superior performance of the MRFO over five other metaheuristic algorithms (i.e., grey wolf optimization, whale optimization, grasshopper optimization, atom search optimization, and salp swarm algorithm) in terms of convergence rate and optimal global solution capture. The entire simulation model is established using MATLAB editor and Simulink. The acquired transient result shows the functionality and viability of the MRFO approach.

INDEX TERMS Optimal control, power system dynamics, MRFO optimization, PV system.

NOMENCLATURE
Variables

a	Ideality constant
a_i	Acceleration
C	Dc-link capacitor
$c_1, c_2, c_3, \vec{r}_1, \vec{r}_2$	Random numbers
d	Drift factor
$\vec{D}, \vec{A}, \vec{C}$	Coefficient vectors
dq0	Direct-quadrature-zero
E_d	Phase voltage of direct-axis
F_i	Reaction force
F_{ij}^i	Interaction force
f_s	Switching frequency
V_{DC_REF}	Reference voltage of dc-link
$V_{DC_{ripple}}$	Ripple voltage

V_{mpp}	Desired maximum voltage
V_t	Array thermal voltage
V_{pv}	Photovoltaic voltage
ω	Synchronous frequency
$\vec{X}_p(k)$	Wolves location
$X_p(t)$	Vector position of the prey

Abbreviations

$h_{ij}(t)$	Height
I	Grid current
I_d	Current in d − axis
$\tilde{\imath}_d$	D − axis errors of current signal
I_o	Array saturation current
$I_{o,c}$	Reverse saturation current
I_{peak}	Peak ac current
I_{pv}	Photocurrent
$I_{pv,c}$	Incident light current
I_q	Current in q − axis

The associate editor coordinating the review of this manuscript and approving it for publication was Bilal Alatas .

$\tilde{i_q}$	Q − axis errors of current signal
I_{q_REF}	Q − axis current reference
k	Boltzmann constant
K_j^1	Location of leader salp
lb_j	Lower boundary
L_f	Interface inductor
M_{best}	Subdivision of the group of atom
M_i	Positon of the food source
N_s	Number of series connected cells
N_p	Number of parallel connected cell
P_{dc}	Active power
$P_{pv}(k)$	Current power
$P_{pv}(k-1)$	Prior measured power
q	Electron charge
R_p	Array equivalent parallel resistance
R_s	Array equivalent series resistance
S_A, S_B, S_C	Switching states
ub_j	Upper boundary
$\hat{V}$	Rms voltage at the pcc
$\widetilde{v_{dc}}$	Voltage error of dc-link
AC	Alternating current
ASO	Atom search optimization
CSA	Cuckoo search algorithm
CF	Cyclone foraging
DC	Direct current
FF	Fitness function
FFO	Fruit fly optimization
GA	Genetic algorithm
GOA	Grasshopper optimization algorithm
GSA	Gravitational search algorithm
GWO	Grey wolf optimization
HSA	Harmony search algorithm
ISE	Integral square error
MPP	Maximum power point
MPPT	Maximum power point technique
P&O	Perturb and Observe
PCC	Point of common coupling
PI	Proportional integral
PID	Proportional integral derivative
MRFO	Manta ray foraging optimization
PV	Photovoltaic
SSA	Salp swarm algorithm
SF	Somersault foraging
WCA	Water cycle algorithm
WOA	Whale optimization algorithm

I. INTRODUCTION

The exponential demand for electricity and the impacts of fossil fuel usage, such as global warming, have resulted in a dramatic increase in renewable energy utilization. Among the sources of renewable energy, photovoltaic (PV) systems have received the greatest attention because of their characteristics of economic incentives, environmental accessibility, and technological advancements [1]. According to market projection, the total installed PV capacity is expected to reach

1.4 TW by 2024 [2], which reflects the level of integrating PV systems into the grid. However, integrating several PV generations into the grid is challenging for power system operation, stability, and reliability. Some control strategies have been adopted to enhance the performance of PV integration into the grid. In [3], a neuro-fuzzy control method was adopted to control the active and reactive power of a grid-connected PV system. Generally, the neuro-fuzzy logic controller is highly adaptable in terms of dealing with a complex and non-linear system without a mathematical model. The fuzzy rules and the neural selection majorly depend on user experience. However, neural network training is time consuming because it requires a large volume of data for an accurate computation. The simple nature of proportional–integral (PI) controller makes it to be highly adopted in PV grid-connected systems [4]. Refs. [5], [6] proposed a PI control method for low-voltage ride through in the grid-connected PV system. In [7], [8], PI controllers were employed to improve the dynamic operation of the PV grid-connected system. The robust stability and tolerance of the distributed generation were improved using multiple input–multiple output for PI controller tuning [9]. While the PI controller can provide wide stability in the control circuit, the PI controller performance is limited to a small load disturbance. Determining the suitable values of the PI controller is very challenging because of non-linearity and parameter variation of PV system. Tuning PI parameters using a trial-and-error method can lead to errors and is time consuming. Alternatively, metaheuristic algorithms have been adopted to obtain accurate PI parameters because of their simplicity, ease of implementation, robustness, and derivative free features. Some of these metaheuristic algorithms reported in the literature to develop the dynamic operation of PV grid-connected system are genetic algorithm (GA) [10], grasshopper optimization algorithm (GOA) [11], harmony search (HS) algorithm [12], cuckoo search algorithm (CSA) [13], fruit fly optimization (FFO) [14], water cycle algorithm (WCA) [15], gravitational search algorithm (GSA) [16], grey wolf optimization (GWO) [17], salp swarm algorithm (SSA)[18], atom search optimization (ASO) [19], and whale optimization algorithm (WOA) [20].

A mathematical model of PV with a proportional–integral derivative (PID) controller optimized using GA was presented in [21]. The GA improved the PID controller performance in relation to reducing rise and overshoot time of the output voltage. Optimal control technique for PV voltage regulation and frequency in microgrid system was presented in [22] using GOA for PI parameter tuning. The author concluded that GOA optimization is a reliable method for solving non-linear systems. The efficacy of HS for tuning multiple cascaded PI controllers in a distributed generation was discussed in [23]. The proposed controller was efficient for effective grid-resynchronizing and islanding operations than the generalized reduced gradient methods and GA. CSA was presented in [24] to enhance the performance of a non-linear grid-tied photovoltaic system. The CSA performance was

TABLE 1. Parameters of the SunPower SPR-305E module at 25 °C and 1000 W/m^2.

I_{mp} (A)	V_{mp} (V)	P_{max} (W)	I_{sc} (A)	V_{oc} (V)	K_v (V/C)	K_I (A/C)	N_{ss} (No)	R_p (Ω)	R_s (Ω)	$I_{o, n}$ (A) $\times 10^{-12}$	a
5.58	54.7	305.226	5.96	64.2	- 0.27269	0.061745	96	269.5934	0.37152	6.3014	0.94504

investigated for multiple PI tuning using artificial neural networks. Consequently, the CSA approach for the non-linear optimization was found to produce a better response. In [25], an improved FFO was employed to enhance the PID controller behaviour. Meanwhile, an automatous micro-grid operation was presented in [26] using WCA to enhance the PI controller parameters. The proposed controller produced a better transient response compared to the genetic algorithm PI-tuned controller. The dynamic performance of GSA for PI controller tuning in a PV grid-connected system was presented in [27]. The results showed that GSA yields better settling time and state error in resolving the grid-connected PV non-linear system. More so, optimal control of a voltage source inverter for an offshore wind farm using the GWO algorithm was presented in [28]. Evidently, [28] showed that a better damped and transient performance is achieved using GWO. The quality improvement of PI parameter for the grid-connected PV system was discussed in [29], [30]. The accuracy, reliability, and efficiency of both frequency and voltage were improved with minimal harmonic distortion using SSA. In addition, [31] proposed ASO to improve the rise time, settling time, and maximum overshoot of a PI controller for DC motor speed controller. An optimal control strategy using WOA was proposed in [32] to optimize the PI parameters in the grid-connected PV system.

The momentous progress of computational algorithm and its potent application in solving non-linear optimization problems have epitomized foremost desire of the authors to employ the Manta ray foraging optimization (MRFO) algorithm to improve the dynamic operation of grid-connected PV system. Power electronic devices such as DC/DC and DC/AC converters are majorly used to regulate the DC voltage of the PV arrays for grid integration. The DC/DC boost converter is employed to trace the maximum power point (MPPT) because of the sensitivity of the PV power to point of operation in the I–V curve. The DC/AC converter is utilized to regulate voltage at the DC-link side and at the point of common coupling (PCC). In this study, the DC/AC and DC/DC converters are controlled using the proposed MRFO algorithm. To the level of the information available to the authors, MRFO has not been applied before to solve any optimization issues in renewable energy. Moreover, the fitness function solution of the MRFO approach developed over the employed algorithms in [32] and [29] motivates the authors to utilize this type of bio-inspired optimization algorithm. The algorithm process depicts foraging characteristics of Manta rays, namely, the chain, cyclone, and summersault techniques, to develop a proficient optimization standard for solving unusual optimization problems. The operation of the MRFO algorithm under distinct operation of the PV system

is extensively compared against the results of WOA, SSA, GWO, GOA, and ASO.

The rest of the paper is organized as follows: Section 2 describes the PV system modelling; Section 3 presents the control strategy of the converters; Section 4 elucidates the problem formulation and the optimization algorithm; Section 5 explains the simulation results; and Section 6 provides the conclusion.

II. MODELING OF THE PV GRID-CONNECTED SYSTEM

The 100 kW PV system comprising of PV arrays, a DC/DC boost converter, a DC bus capacitor, a maximum power point tracking unit, a two-level DC/AC bidirectional converter with a control unit, a filter, transmission lines, and step-up transformers (Fig. 1) was used to study the MRFO performance. Each PV module had a 305.2W_p rating. The PV arrays were arranged in 66 strings, with each string made up of five modules in series (66 × 5 × 305.2 W= 100.7 kW). The description of the design model is illustrated in following subsection.

A. MODELING OF PV ARRAYS AND MPPT CONTROL

The equivalent model of PV array is shown in Fig. 2. This comprise of several modules made of several cells. The mathematical model of the PV array is depicted as [34]:

$$I = I_{pv} - I_0 \left[\exp\left(\frac{V + R_sI}{aV_t} \right) - 1 \right] - \frac{V + R_sI}{R_p} \quad (1)$$

where $I_{pv} = N_pI_{pv,c}$ is the array photocurrent; $I_{pv,c}$ is the incident light current; N_p is the number of parallel connected cells; $I_o = N_pI_{o,c}$ is the array saturation current; $I_{o,c}$ is the reverse saturation current of the diode; $V_t = N_sKT/q$ is the array thermal voltage; T is temperature of the cell; q is the electron charge; a is the ideality constant of the diode; R_s is the array equivalent series resistance; R_p is the array equivalent parallel resistance; N_s is the number of cells in series; and k is Boltzmann constant. Table 1 describes the parameters of the SunPower SPR-305E-WHT-DPV array ($S_{series} = 5$ and $P_{parallel} = 66$) used for the MATLAB/Simulink simulation. Fig. 3 describes typical I–V and P–V curve of the PV array obtained using (1) array under changing irradiation.

B. MAXIMUM POWER POINT TRACKING ALGORITHM

The PV output power varies because of the changing temperature and irradiance. As a result, the maximum power point (MPP) from the PV system is extracted using the MPPT algorithm. The MPPT algorithm, called Perturb and Observe (P&O), utilized for the simulation purposes.
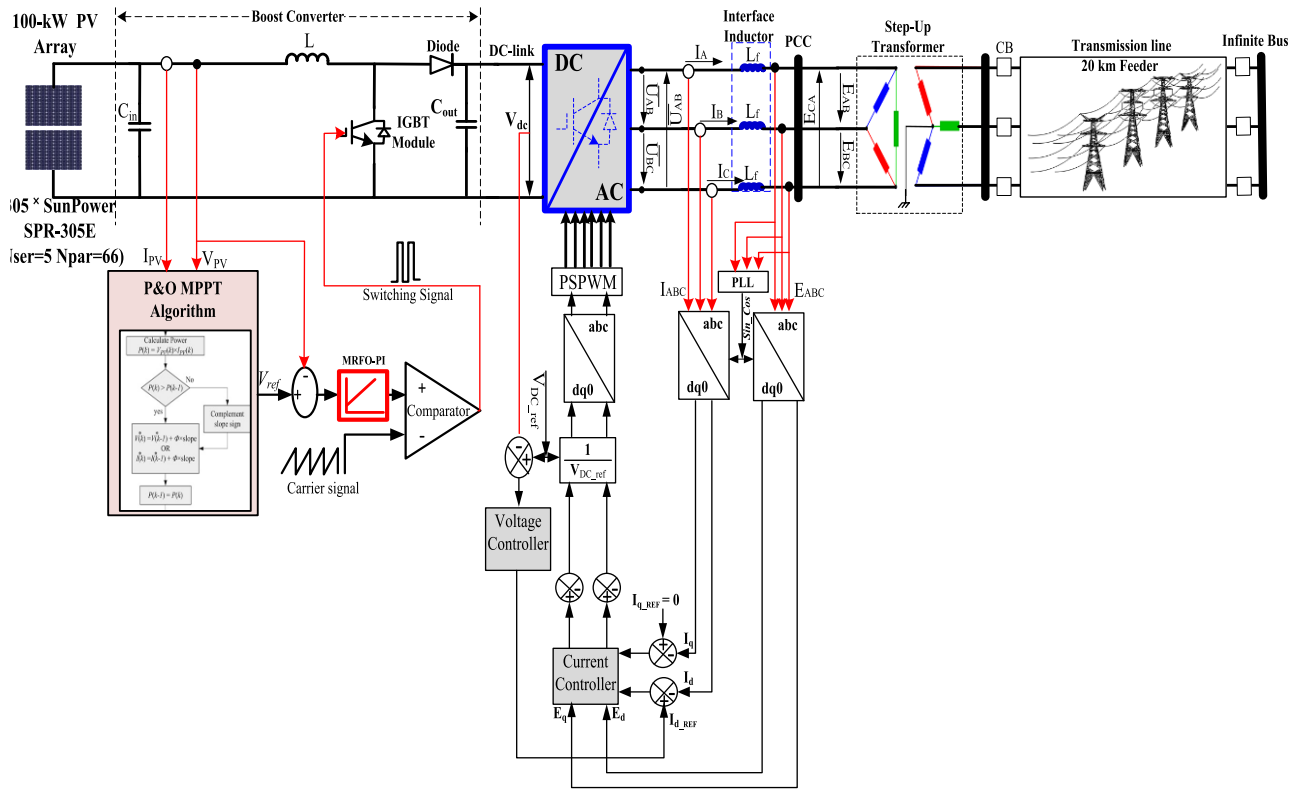
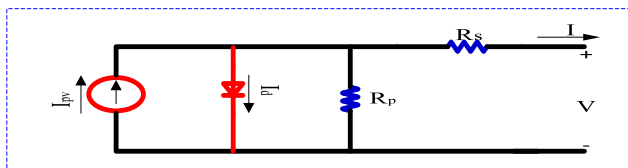**FIGURE 1.** Overall PV grid-connected structure.

FIGURE 2. PV array corresponding model [35].

The instantaneous current and voltage values were measured and recorded in a specific amount of time. A small amount of perturbation was added to the reference voltage with a constant step size in each specific time. The increases in the output power with respect to the increase in reference implied that the system was coming near the MPP. Therefore, the perturbation track must be kept along the same route or, else, the perturbation will move in the reverse direction. Consequently, the PV system may possibly arrive at a swinging point near the real MPP [35]. The mathematical description of the P&O algorithm [36] is represented as follows:

$$\frac{dP_{pv}(k)}{dV_{pv}(k)} = \frac{P_{pv}(k) - P_{pv}(k-1)}{V_{pv}(k) - V_{pv}(k-1)} \qquad (2)$$

where $P_{pv}(k)$, $P_{pv}(k-1)$, $V_{pv}(k)$, and $V_{pv}(k-1)$ represent the current power, prior measured power, current PV voltage, and prior voltage, respectively.

III. CONTROL STRATEGY OF THE DC/DC AND DC/AC CONVERTERS

A. DC/DC BOOST CONVERTER

The DC/DC boost converter was implemented in this study to realize MPPT operating point by adjusting the duty cycle (D). Stepping-up the input voltage magnitude to a desired operating value for load connection requires a boost converter. An ideal replication of the DC/DC boost converter comprises a high-frequency switch, an inductor, a diode, an output filtering capacitor, an MPPT algorithm, a high-frequency carrier signal, a high-speed comparator, and a PI controller (Fig. 4). The DC/DC converter parameters were picked to make the converter operate in a continuous conduction mode. Table 2 describes the simulation parameters of the DC/DC boost converter. The output power was sent to the MPPT algorithm, which consequently produced the duct cycle (D). The DC/DC converter operation was controlled by the value of D that will produce the desired voltage (V_{mpp}).

B. DC/AC CONVERTER

The utmost purpose of the MRFO-based controller algorithm is to generate active power for the grid at the PCC.

This was attained by producing reference currents from the DC links through the DC/AC converter. From Fig. 1, the equivalent abc frame at the PCC is represented as follows
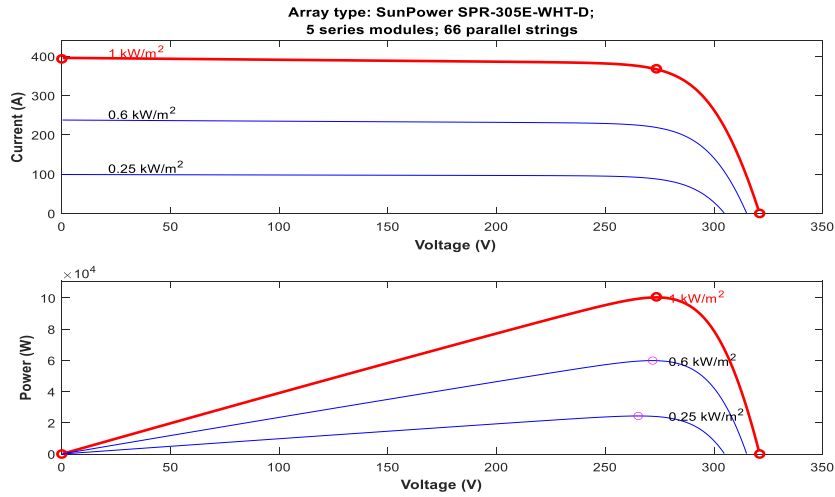
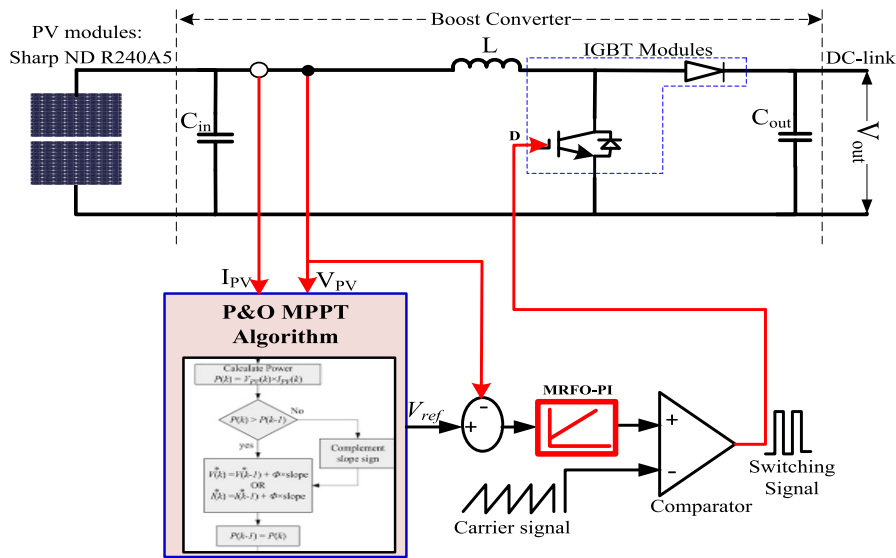**FIGURE 3.** I–V and P–V curves of the SunPower SPR-305E PV array.

FIGURE 4. DC/DC boost converter.

by using Kirchhoff's current and voltage:

$$\begin{bmatrix} E_{AO'} \\ E_{BO'} \\ E_{CO'} \end{bmatrix} = \begin{bmatrix} \overline{U_{AO}} \\ \overline{U_{BO}} \\ \overline{U_{CO}} \end{bmatrix} + L_f \frac{d}{dt} \begin{bmatrix} I_A \\ I_B \\ I_C \end{bmatrix} + U_{O'O} \quad (3)$$

$$C \frac{dV_{dc}}{dt} = \begin{bmatrix} S_A & S_B & S_C \end{bmatrix} \begin{bmatrix} I_A \\ I_B \\ I_C \end{bmatrix} \quad (4)$$

where L_f is the interface inductor; C is the DC-link capacitor; S_A, S_B, and S_C represent the balance conditions of the model under its switching states; and $U_{O'O}$ is the voltage between the grid neutral point (O') and the neutral virtual point from the corresponding circuit model (O).

The inductor L_f can be expressed as [37]

$$\frac{5V_{dc}}{16f_s I_a} \leq L_f \leq \sqrt{\frac{0.5V_{dc}^2 - 220^2}{I * \omega}} \quad (5)$$

where I, V_{dc}, f_s, and ω are the grid current RMS value, DC-link voltage, switching frequency, and angular frequency, respectively.

The DC-link capacitor is expressed as:

$$C = \frac{0.9I_{peak}}{4\sqrt{2}\pi f V_{DC_{ripple}}} \quad (6)$$

where I_{peak}, f, and $V_{DC_{ripple}}$ are the peak AC current, grid frequency, and permissible ripple voltage of the DC link, respectively.

TABLE 2. Optimization parameters.

Parameters	Values
Maximum Iteration	200
Population size	50
Upper boundary	10, 1000, 5, 50, 5, 50
Lower boundary	0,0,0,0,0,0
Dimension	6
Input capacitance (C_{in})	$100\mu F$
Boost converter inductance (L)	5mH
Output Capacitance (C_{out})	6mF
Maximum PV output power	100kW
Voltage at maximum power point	54.7 V
Current at maximum power point	5.58A
Number of modules in parallel	13
Number of modules in series	5
DC bus voltage	500V
Frequency	60Hz
Filter (L_f)	$760\mu H$
AC Voltage (L − L)	260V
Transformer Y/Δ	20/0.26kV

By assuming, a balanced voltage, the voltage between the neutral virtual point of the corresponding circuit model (O) and the grid neutral point (O') is represented as:

$$U_{O'O} = -\frac{(\overline{U_{AO}} + \overline{U_{BO}} + \overline{U_{CO}})}{3} \quad (7)$$

$$\begin{bmatrix} \overline{U_{AO}} \\ \overline{U_{BO}} \\ \overline{U_{CO}} \end{bmatrix} = V_{dc} \begin{bmatrix} S_A \\ S_B \\ S_C \end{bmatrix} \quad (8)$$

The following relation is obtained by substituting (8) into (3) and (4):

$$\frac{d}{dt} \begin{bmatrix} I_A \\ I_B \\ I_C \end{bmatrix} = \frac{1}{L_f} \begin{bmatrix} E_{AO'} \\ E_{BO'} \\ E_{CO'} \end{bmatrix} - \frac{V_{dc}}{L_f} \left(\begin{bmatrix} S_A \\ S_B \\ S_C \end{bmatrix} - \frac{1}{3} \begin{bmatrix} S_A & S_B & S_C \end{bmatrix} \begin{bmatrix} 1 \\ 1 \\ 1 \end{bmatrix} \right) \quad (9)$$

Equation (9) represents the equivalent dynamic model of DC/AC converter used in abc frame. The switching state functions, $d_i(i = A, B, C)$, are denoted as follows:

$$\begin{bmatrix} d_A \\ d_B \\ d_C \end{bmatrix} = \left(\begin{bmatrix} S_A \\ S_B \\ S_C \end{bmatrix} - \frac{1}{3} \begin{bmatrix} S_A & S_B & S_C \end{bmatrix} \begin{bmatrix} 1 \\ 1 \\ 1 \end{bmatrix} \right) \quad (10)$$

By combining (9) and (10), the equivalent dynamic of the circuit model in the abc frame is represented as

$$L_f \frac{d}{dt} \begin{bmatrix} I_A \\ I_B \\ I_C \end{bmatrix} = \begin{bmatrix} E_{AO'} \\ E_{BO'} \\ E_{CO'} \end{bmatrix} - V_{dc} \begin{bmatrix} d_A \\ d_B \\ d_C \end{bmatrix} \quad (11)$$

The differential equation of the DC side is given as

$$\frac{dV_{dc}}{dt} = \frac{1}{C}I_{dc} = \begin{bmatrix} d_A & d_B & d_C \end{bmatrix} \begin{bmatrix} I_A \\ I_B \\ I_C \end{bmatrix} \quad (12)$$

$$\frac{dV_{dc}}{dt} = \frac{1}{C}(2d_A + d_B)I_A + \frac{1}{C}(d_A + 2d_B)I_B \quad (13)$$

Equations (11) and (13) showed that the model is time-dependent. Therefore, the model is represented with a constant frequency ω rotating in the synchronous reference frame to simplify the implementation of the MRFO control algorithm. The corresponding transformation matrix is

$$C_{dq}^{abc} = \sqrt{\frac{2}{3}} \begin{bmatrix} \cos\theta & \cos(\theta - 2\pi/3) & \cos(\theta - 4\pi/3) \\ -\sin\theta & -\sin(\theta - 2\pi/3) & -\sin(\theta - 4\pi/3) \end{bmatrix} \quad (14)$$

where $\theta = \omega t$.

Eq. (15) is achieved by applying coordinate transformation to Eq. (12):

$$L_f \frac{d}{dt} \begin{bmatrix} I_d \\ I_q \end{bmatrix} = \begin{bmatrix} E_d \\ E_q \end{bmatrix} + L_f\omega \begin{bmatrix} I_q \\ -I_d \end{bmatrix} - V_{dc} \begin{bmatrix} d_d \\ d_q \end{bmatrix} \quad (15)$$

In the same manner, Eq. (16) can be obtained by relating this transformation to Eq. (12):

$$C\frac{dV_{dc}}{dt} = d_d I_d + d_q I_q \quad (16)$$

The obtained model in Eqs. (15) and (16) is non-linear because of the multiplication between the state variables (i.e., I_d, I_q, and V_{DC}) and input (i.e., d_d and d_q).

Figure 6 shows the DC/AC converter control schematic diagram. Only two phase currents were evaluated because the proposed system was a three-wire configuration. Currents I_d and I_q were obtained by measuring and converting I_A and I_B to dq0. Therefore, Eq. (15) is modified as follows:

$$L_f \begin{bmatrix} u_d \\ u_q \end{bmatrix} = \begin{bmatrix} E_d \\ E_q \end{bmatrix} + L_f\omega \begin{bmatrix} I_q \\ -I_d \end{bmatrix} - V_{dc} \begin{bmatrix} d_d \\ d_q \end{bmatrix} \quad (17)$$

where $\begin{bmatrix} u_d \\ u_q \end{bmatrix} = \frac{d}{dt} \begin{bmatrix} I_d \\ I_q \end{bmatrix}$.

Equation (18) shows that input u_d and u_q can be used to control the I_d and I_q currents independently. Hence, the following expression is used to design the controller:

$$u_d = k_p \widetilde{i_d} + k_i \int \widetilde{i_d} dt$$

$$u_q = k_p \widetilde{i_q} + k_i \int \widetilde{i_q} dt \quad (18)$$

where $\widetilde{i_d} = I_{d\_REF} - I_d$ and $\widetilde{i_q} = I_{q\_REF} - I_q$ are the errors of the current signal, with I_{d_REF} and I_{q_REF} as the current reference values for I_d and I_q, respectively.
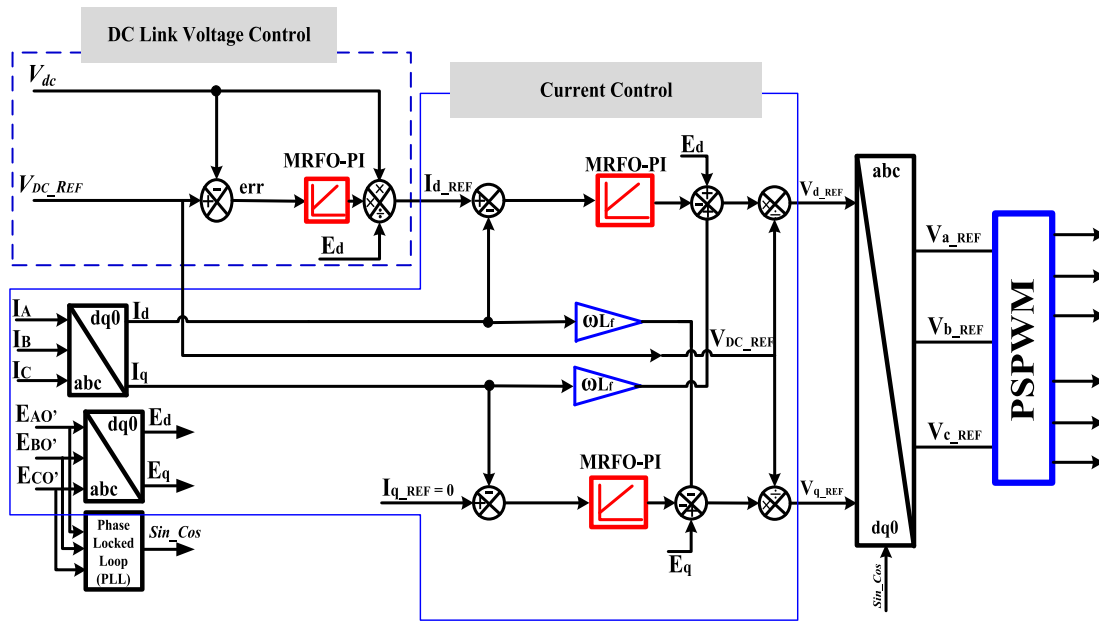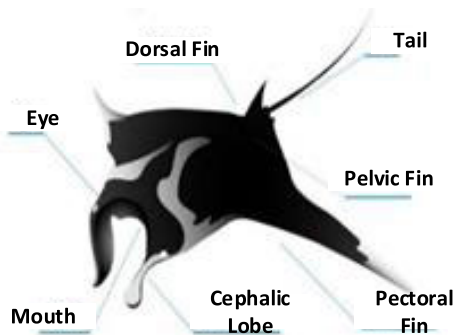
FIGURE 5. DC/AC MRFO-PI control block diagram.

FIGURE 6. Anatomy of a manta ray.

From Eq. (17), the current control can be represented with the following equation:

$$\begin{bmatrix} d_d \\ d_q \end{bmatrix} = \frac{L_f \omega}{V_{dc}} \begin{bmatrix} I_q \\ -I_d \end{bmatrix} + \frac{1}{V_{dc}} \begin{bmatrix} E_d \\ E_q \end{bmatrix} - \frac{L_f}{V_{dc}} \begin{bmatrix} u_d \\ u_q \end{bmatrix} \quad (19)$$

The d-axis is used to adjust the active power. The reference current value, I_{d_REF}, is generated through the DC-link voltage controller. The load q-axis is used to regulate the reactive power. Current (I_{Lq}) represents I_{q_REF}, which is the q-axis reference current. A unity power factor can be obtained by forcing $i_{q\_REF} = 0$. The power derivation for controlling the active power is a proportional direct-axis current I_d and represented as:

$$P_{dc} = \frac{3}{2} \left(E_d I_d + E_q I_q \right) = \frac{3}{2} E_d I_d \quad (20)$$

Eq. (20) evidently shows that operating the DC-link voltage at a desire level requires the direct-axis current I_d.

Thus, using Eq. (16), it is given as

$$C \frac{dV_{dc}}{dt} = d_d I_d = u_{dc} \quad (21)$$

Consequently, the active current is obtained as

$$I_d = \frac{u_{dc}}{d_d} = \frac{u_{dc} V_{dc}}{d_d V_{dc}} \quad (22)$$

The following equation for a perfect current loop and balance system operating condition holds:

$$d_d V_{dc} = E_d \quad (23)$$

$$I_d = \frac{u_{dc}}{d_d} = \frac{u_{dc} V_{dc}}{E_d} \quad (24)$$

$$\begin{bmatrix} E_d \\ E_q \end{bmatrix} = \sqrt{\frac{3}{2}} \begin{bmatrix} \hat{V} \\ 0 \end{bmatrix} \quad (25)$$

where E_d is phase voltage of the direct axis and $\hat{V}$. is the RMS voltage at the PCC. Consequently, the loop voltage of the DC link is controlled using

$$I_{d\_REF} = \frac{u_{dc}}{d_d} = \sqrt{\frac{2}{3}} \frac{V_{dc}}{\hat{V}} u_{dc} \quad (26)$$

The DC-link voltage is controlled with the use of PI controller and it is expressed as:

$$u_{dc} = k_{pdc} \widetilde{v_{dc}} + k_{idc} \int \widetilde{v_{dc}} dt \quad (27)$$

where $\widetilde{v_{dc}} = V_{DC\_REF} - V_{dc}$ is the voltage error of the DC-link, while V_{DC_REF} and V_{dc} are the reference voltage of the DC-link and the average voltage, respectively. The difference between the voltage reference of the DC-link and the sum of the real DC-link voltages is sent to the PI controller such that the control parameter u_{dc} can be estimated (Fig. 5).

IV. PROBLEM FORMULATION AND OPTIMIZATION METHOD

Fig. 4 and 5 show the block diagram for calculating the PI controller parameters, where "err" denotes the difference between the output and input signals. The optimization process commences by suppling the initial values as the controller parameters. The optimization stops when the minimum value is obtained. The optimum PI parameters were achieved when the calculated fitness function (FF) produced the minimum value that resulted into the best transient response of the studied PV grid-connected system. As shown in (28), the integral square error (ISE) was used to determine the appropriate FF to obtain the controller parameters. The MRFO code with the selected number of variables (PI parameters), FF, particles, and number of iterations was implemented using a MATLAB/Simulink editor, while the proposed PV system was developed in MATLAB/Simulink. The ISE value was calculated in Simulink before being sent to the MATLAB workspace, where the MRFO was utilized to minimize the FF. Finally, the optimized PI parameters were inserted into the Simulink design when the maximum level of iteration was reached to obtain the appropriate transient behavior of the grid-connected PV system.

$$\text{ISE} = \int_0^\infty e^2(t)\,dt \tag{28}$$

The MRFO effectiveness and performance were evaluated with respect to five well-established metaheuristic algorithms: WOA, SSA, GWO, GOA, and ASO.

A. WOA

The WOA is a unique nature-inspired metaheuristic algorithm, which imitates the social activities of humpback whales. The WOA was developed based on the search for prey, which is characterized by encircling and bubble-net foraging behavior of humpback whales. During a search operation, humpback whales dive to chase prey, thereby creating a spiral shape to simulate bubble attacking strategy round the prey. During this maneuvering, the humpback whale swims to the surface. The WOA is majorly models based on encircling, bubble attack, and searching for the prey [20]. In WOA, the position of prey is regarded as a feasible solution. The following equation represents the en'circling of prey:

$$D = |C \cdot X_p(t) - X(t)|$$
$$X(t+1) = X_p(t) - A \cdot D$$
$$A = 2a \cdot r - a$$
$$C = 2 \cdot r \tag{29}$$

where $X(t)$ is the vector position of whales; t depicts the present iteration; $X_p(t)$ is the vector position of the prey, where the coefficient vector is represented as A and C; r represents a random vector which is between 0 and 1; and vector "a" is progressively from 2 to 0.

The bubble behavior of whales is usually described in two ways:

  i Shrinking encircling mechanism: Whales form shrinking circles to swim from place to place round the prey, which is realized by reducing "a" starting from 2 to 0 alongside the iterations and $|A| < 1$.

 ii. Updating of position through spiraling: The humpback whales form a spiral shape to swim to the prey. The mathematical equation for this is

$$X(t+1) = D' \cdot e^{bl} \cdot \cos(2\pi l) + X_p(t) \tag{30}$$
$$D' = |X_p(t) - X(t)| \tag{31}$$

where b is a constant defining the spiral logarithmic form, and l is a random number within $[-1\ 1]$. Whales perform the two methods concurrently during the attacking procedure. The probability model of the spiral positon is represented as

$$X(t+1) = \begin{cases} X_p(t.) - A \cdot D & \text{if } p < 0.5 \\ D' \cdot e^{bl} \cdot \cos(2\pi l) + X_p(t) & \text{if } \geq 0.5 \end{cases} \tag{32}$$

where p is a random number in $|0, 1|$.

The global search for a prey by humpback whales is modeled in the equation below. $|A| > 1$ can conveniently express the searching process.

$$D = |C \cdot X_r(t) - X(t)| \tag{33}$$
$$X(t+1) = X_r(t) - A \cdot D \tag{34}$$

B. SSA

Salps are a family of Salpidae with a barrel-shaped transparent body. Their movement is similar to that of jellyfish (i.e., pumping water to move forward). Similar to other bio-inspired algorithms, the location of the exploration agent starts with a random value as shown below [18]:

$$K_1^{1:n} = \text{rand} \cdot (ub_j - lb_j) + lb_j, \quad \forall j \in \text{no. of varables} \tag{35}$$

where $K_1^{1:n}$ denotes the first position of the salps; ub_j and lb_j denote the upper and lower boundaries, respectively; and rand is used to generate a random number within $[0\ 1]$.

A salp swarm is separated into dual distinct factions: followers and leaders. The leaders direct the swarm, while the followers follow the pursuit for the represented food area progressively. The number of parameters to be controlled is represented as an *n* dimension equivalent to the position of individual salp in the hunt space. Likewise, the position of the whole amount of salps is stored in in the matrix as follows [18]:

$$K_j^1 = \begin{cases} M_i + 2e^{-\left(\frac{4l}{L}\right)^2}\left((ub_j - lb_j)c_2 + lb_j\right), & c_3 \geq 0, \\ M_i - 2e^{-\left(\frac{4l}{L}\right)^2}\left((ub_j - lb_j)c_2 + lb_j\right), & c_3 < 0, \end{cases} \tag{36}$$

where K_j^1 stands for the location of the leader salp in the jth dimension; M_i indicates the position of the food source in the jth dimension, and the random numbers are c_1, c_2, and c_3;

L is the number of maximum iteration; and l represents the current iteration.

Equation (37) is used to update the location of the salp followers, which is similar to Newton's law of motion.

$$K_j^i = \frac{1}{2}at^2 + v_o t \qquad (37)$$

where K_j^i is the location of the ith follower salp in the jth dimension, and $i \geq 2$. v_o is the optimization velocity at the beginning of the optimization process selected as zero.

C. GWO

The GWO is a natured inspired algorithm that imitates the guidance pyramid and hunting behavior of grey wolves in nature. The hunting mechanism of grey wolves comprises three steps: searching for prey, encircling the prey, and attacking the prey. Grey wolves regularly reside in groups and are arranged into four representatives. The α wolves are the leader; the β wolves support α in obligations and can substitute α if they die; the δ wolves are the hunters, keepers, and explorers of the cluster; and ω wolves attend to the young group members [17].

The mathematical model based on the GWO social hierarchy is considered on the premise of α as the first best solution and β and δ as the second and third solutions, respectively. Grey wolves usually encircle their prey when they hunt. Equation (38) describes the mathematical equation to represent this behavior.

$$\vec{D} = \left| \vec{C} \cdot \vec{X}_p(k) - \vec{X}(k) \right|$$
$$\vec{X}(k+1) = \vec{X}_p(k) - \vec{A} \cdot \vec{D}$$
$$\vec{A} = 2\vec{a} \cdot \vec{r}_1 - \vec{a}$$
$$\vec{C} = 2 \cdot \vec{r}_2 \qquad (38)$$

where $\vec{D}$, $\vec{A}$, and $\vec{C}$ are coefficient constants; k is the recent iteration; $\vec{X}(k)$ is the prey location; and $\vec{X}_p(k)$ is the wolves' location. $\vec{r}_1$ and $\vec{r}_2$ are random numbers between [0, 1]. The $\vec{a}$ values are linearly decreased from 2 to 0.

The hunting process is modeled according to the ability of the α, β, and δ wolves to locate preys and encircle them. Therefore, the first three finest solutions are kept, and this mandates other searching wolves to update their location. Equation (39) represents this type of behavior.

$$\vec{D}_{\alpha,\beta,\delta} = \left| \vec{C}_{1,2,3} \cdot \vec{X}_{\alpha,\beta,\delta} - \vec{X} \right|$$
$$\vec{X}_{1,2,3} = \vec{X}_{\alpha,\beta,\delta} - \vec{A}_{1,2,3} \cdot \vec{D}_{\alpha,\beta,\delta}$$
$$\vec{X}(k+1) = \frac{\vec{X}_1 + \vec{X}_2 + \vec{X}_3}{3} \qquad (39)$$

The exploration of the GWO algorithm is formulated from the location of the α, β, and δ wolves. The wolves start far away from one another and progressively move nearer to attack the prey and encircle them. This is depicted according to $\left| \vec{A} \right| > 1$, which forces the wolves to find the prey.

D. GOA

The GOA is mathematically modeled based on the swarming behavior of grasshoppers for solving optimization challenges. To depict the social behavior of grasshoppers in nature, attraction and repulsion forces are used to link grasshoppers with their next position. The attraction force allows grasshoppers to perform a local search, while the repulsion force allows grasshoppers to perform a global search. GOA is fortified with a constant that decreases the comfort zone of the grasshoppers to enable a balanced search between these two processes. As a result, the best value acquired so far by the swarm is deliberated as a target to be hunted and improved by the grasshoppers along the direction of the target. The d− dimensional position of the ith grasshopper can be mathematically represented as follows by denoting the total grasshopper as G in the swarm [38]:

$$X_i^d(t+1) = \sum_{\substack{j=1 \\ j \neq i}}^{G} \frac{ub_d - lb_d}{2} c(t) s(r) \left(\left| x_j^d(t) \right. \right.$$
$$\left. \left. - x_i^d(t) \right| \right) \frac{x_j(t) - x_i(t)}{d_{ij}} + \widehat{T}_d$$
$$s(r) = f \cdot \exp\left(\frac{-r}{l} \right) - \exp(-r)$$
$$c(t) = c_{max} - t \frac{c_{max} - c_{min}}{t_{max}} \qquad (40)$$

where t is the present iteration; s is used to decide the strength of attraction forces and reputation; f defines the intensity of attraction; l is the attractive length scale; lb_d and ub_d are the lower and upper boundaries in the d-dimensional space, respectively; d_{ij} is the distance between the ith and jth grasshoppers; and $\widehat{T}_d$ is the best d-dimensional location; c is the decreasing factor for achieving an equilibrium between exploitation and exploration. The larger the value of c, the wider the exploration. The smaller the value, the smaller the exploitation in GOA.

E. ASO

ASO is a physics-inspired metaheuristic optimization algorithm based on molecular forces used to mathematically depict the atomic movement for problem optimization. This algorithm is based on constraint and interaction forces. The ASO atomic movement obeys Newton's second law of motion. The repulsive forces allow the atoms to exploit the target region adequately, while the attractive force allows the atoms to explore the search region expansively. From Newton's second law, if c_i is the constraint force of an atom, and F_i is the reaction force, the acceleration with mass is represented as [39]

$$a_i = \frac{F_i + C_i}{m_i} \qquad (41)$$

Lennard-Jones' (L − J) potential equation is represented as follows:

$$F_{ij}^i = -\alpha \left(1 - \frac{t-1}{T}\right)^3 e^{\frac{20t}{T}} \left(2h_{ij}(t)^{13} - h_{ij}(t)^7\right) \quad (42)$$

where F_{ij}^i is the interaction force acting on the ith atom from the jth atom in the dth dimension in time t; and α and T are the depth weight and maximum iterations, respectively. The height of F with different $\eta(t)$ values is depicted in Eq. (43) as

$$h_{ij}(t) = \begin{cases} h_{min} = d_o + d(t), & \frac{r_g(t)}{\sigma(t)} < h_{min} \\ \frac{r_g(t)}{\sigma(t)}, & h_{min} \leq \frac{r_g(t)}{\sigma(t)} \leq h_{max} \\ h_{max} = u, & \frac{r_y}{\sigma(t)} > h_{max} \end{cases}$$

$$\sigma(t) = \left\| x_g(t), \frac{\sum_{j \in M_{best}} x_{ij}(t)}{M(t)} \right\| \quad (43)$$

where M_{best} is a subdivision of the group of atoms, which contains the firstM atoms with the optimal FF values, and d is the drift factor for reconnecting the algorithm to utilization presented as

$$d(t) = \frac{1}{10} \sin\left(\frac{\pi t}{2T}\right) \quad (44)$$

The ith atom constraints are

$$\theta_i(t) = \left[|p_i(t) - p_{best}(t)|^2 - b_{i,best}^2 \right] \quad (45)$$

where the location of the best atom is denoted as $p_{best}(t)$ at the tth iteration, and $b_{i,best}$ is the fixed bond length linking the best atom and the ith atom. Therefore, the constraint force modification is represented as

$$G_i^d(t) = \beta e^{\frac{20t}{T}} \left(p_{best}^d(t) - p_i^d(t)\right) \quad (46)$$

F. MRFO

Manta rays are a family of large rays classified under the Manta genus. These creatures possess fleshy pectoral fins that resemble wings projecting as cephalic fins from the head to the large forward-facing mouth (Fig. 6). They possess different and excellent foraging strategies to feed on planktons, including the chain, somersault, and cyclone foraging techniques (Fig. 7). MRFO is a bio-inspired optimization algorithm, and its conduct depicts three foraging characteristics of Manta rays for developing a proficient optimization standard for solving unusual optimization problems [33].

1) CHAIN FORAGING

The first stage of foraging in MRFO involves chain foraging techniques. When numerous Manta rays commence foraging, they form an orderly connection behind one another. The smaller males are piggybacked by females by swimming to balance the beat of the pectoral fins of the females. As a result, the ones behind will pick a plankton missed by the previous Manta rays. This level of cooperation will result into channeling large quantities of plankton into their gills,
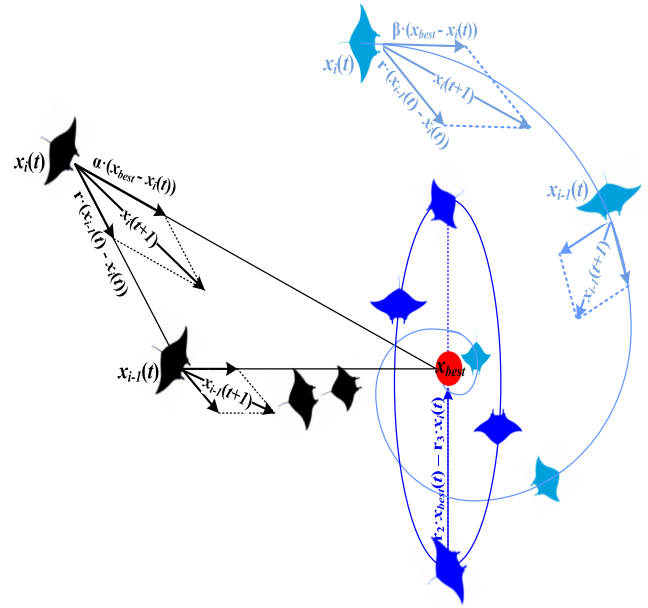

FIGURE 7. Foraging behaviors of the manta rays (black: Chain foraging; light blue: Cyclone foraging; blue: Somersault foraging; red: Plankton with high concentration.

which will increase their food consumption. The greater the quantities of plankton in a place, the virtuous the place is likely to be. However, this is not the best solution. MRFO believes that the finest solution so far is the location with the highest plankton. The chain foraging mathematical model is depicted as [33]:

$$x_i^d(t+1)$$
$$= \begin{cases} x_i^d(t) + r \cdot \left(x_{best}^d(t) - x_i^d(t)\right) + a \cdot \left(x_{best}^d(t) - x_i^d(t)\right) \\ \qquad i = 1 \\ x_i^d(t) + r \cdot \left(x_{i-1}^d(t) - x_i^d(t)\right) + a \cdot \left(x_{best}^d(t) - x_i^d(t)\right) \\ \qquad i = 2, \dots N \end{cases}$$
$$\quad (47)$$

$$a = 2r \cdot \sqrt{|\log(r)|} \quad (48)$$

where x_i^d is the location of ith individual at time t in the dth dimension; a is a weight coefficient; r is a random number between [0, 1]; and $x_{best}^d(t)$ is the high-concentration plankton.

2) CYCLONE FORAGING

In cyclone foraging (CF), once a group of Manta rays discovers a spot of plankton in deep water, they will swim close to the food by spiraling after establishing a long forage chain. Along with the spiraling technique, every Manta ray will then swim in the direction of food ahead of each individual. In essence, each Manta ray not only follows the food ahead of it, but also travels in the direction of food in a spiraling manner. The equation below depicts the CF of Manta rays in

the search region [33]:

$$
x_i^d(t+1)
= \begin{cases}
x_{best}^d + r \cdot \left(x_{best}^d(t) - x_i^d(t)\right) + \beta \cdot \left(x_{best}^d(t) - x_i^d(t)\right) \\
\qquad i = 1 \\
x_{best}^d + r \cdot \left(x_{i-1}^d(t) - x_i^d(t)\right) + \beta \cdot \left(x_{best}^d(t) - x_i^d(t)\right) \\
\qquad i = 2, \ldots N
\end{cases}
\tag{49}
$$

$$
\beta = 2e^{r_1 \frac{T-t+1}{T}} \cdot \sin(2\pi r_1)
\tag{50}
$$

where β represents the weight constant; r_1 is the rand number between [0, 1]; and T denotes the maximum iterations.

Manta rays can be forced to explore for a different food target far away from existing feasible food targets by allocating a new random location in the whole searching area as the target position. This method primarily emphasizes the exploration and allows the MRFO to attain a far-reaching global search. The CF mathematical model is presented as follows [33]:

$$
x_{rand}^d = Lb^d + r \cdot \left(Ub^d - Lb^d\right)
\tag{51}
$$

$$
x_i^d(t+1)
= \begin{cases}
x_{rand}^d + r \cdot \left(x_{rand}^d - x_i^d(t)\right) + \beta \cdot \left(x_{rand}^d - x_i^d(t)\right) \\
\qquad i = 1 \\
x_{rand}^d + r \cdot \left(x_{i-1}^d(t) - x_i^d(t)\right) + \beta \cdot \left(x_{rand}^d - x_i^d(t)\right) \\
\qquad i = 2, \ldots N
\end{cases}
\tag{52}
$$

where x_{rand}^d is a random position, and Ub^d and Lb^d are the upper and lower limits of the dimensions, respectively.

3) SOMERSAULT FORAGING (SF)

Each Manta ray will endeavour to swim back and forth from one place to another round the pivot and somersault to another location. As a result, Manta rays will update their locations around the best location obtained so far. The SF mathematical model is presented as follows [33]:

$$
x_i^d(t+1) = x_i^d(t) + S \cdot \left(r_2 \cdot x_{best}^d - r_3 \cdot x_i^d(t)\right) \quad i = 1, \ldots N
\tag{53}
$$

where S represents the somersault constant, and r_2 and r_3 are random numbers between [0, 1]. Fig. 8 shows the MRFO flowchart.

V. SIMULATION RESULTS

The complete model and dynamic response of an MRFO-based PI grid-connected PV system have been presented in this study. The simulation was accomplished using MATLAB editor and Simulink. A variable time step of 5e-6 was used to obtain a good response of the proposed system. The performance of the MRFO-based PI controller was evaluated in relation to the dynamic response when subjected to a varying irradiance (Fig. 9) at 25 °C constant temperature.
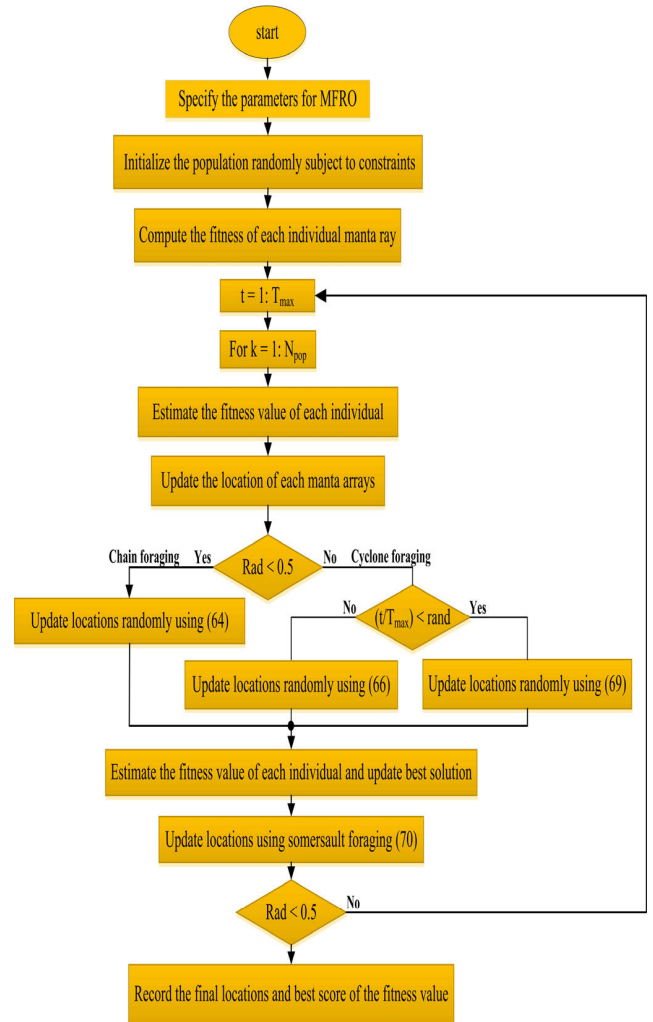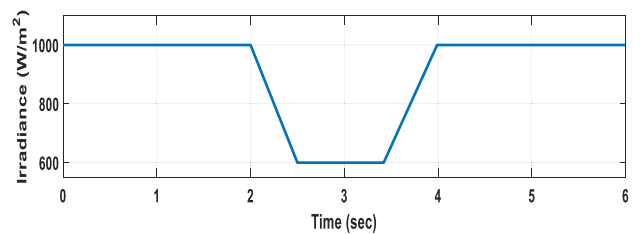

FIGURE 8. MRFO flowchart.

FIGURE 9. Fast dropping and rising irradiance.

This is compared with the performance of GOA, WOA, ASO, GWO and SSA algorithms under same system parameters (Table 2). The variable of the optimization problem was selected as the proportional and integral gain of the PI controller for the DC/DC and DC/AC converters.

One significant criterion for assessing the performance of any optimization method is the evaluation of their convergence rate. Therefore, all algorithms were subjected to minimize FF with the same number of iterations, boundary conditions, and search agents (Table 2) for rational
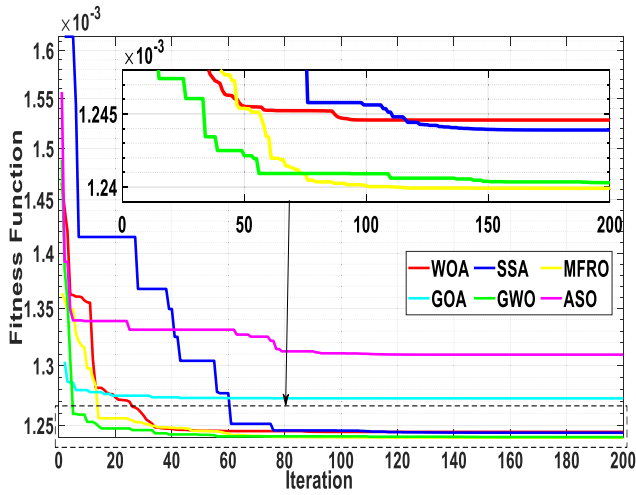
FIGURE 10. Convergence curves of all algorithms.

comparison. Fig. 10 shows the convergence curves of all six selected algorithms. The figure reveals that the MRFO performs well compared with the five meta-heuristic algorithms in terms of convergence speed and optimal solution capture.

The minimization of the integral error was required; hence, the curve with a minimum ISE optimization value was selected. Convergence curves are generally evaluated based on two main parameters: maximized value or minimized value of the FF and the convergence speed. The former provides information on quality of the solution obtained by the optimization algorithms, while the latter gives information on the speed of the convergence curve. Table 3 lists the values for the solution quality and the convergence rate obtained from Fig. 10.

TABLE 3. Optimal values of the six algorithms.

Algorithm	Fitness Function (FF)	FF iteration
GOA	0.00127236906	33
GWO	0.00124029608	148
WOA	0.00124457692	93
ASO	0.00130955350	92
SSA	0.00124389569	140
MRFO	0.00123991830	100

Fig. 10 and Table 3 depict that the MRFO had a better-quality solution with a good convergence speed, whereas the other algorithms exhibited low-quality solutions with a premature convergence. At the start of the simulation, each optimization algorithm commenced its searching procedure for the best probable PI parameter combination that offers best response for the system. The optimization process stopped when the required number of iterations were completed. The results can be fetched from the MATLAB workspace.

Table 4 presents finest values of the PI parameters by the six algorithms for 200 iterations.

As discussed in Section 1, connecting the PV with the grid requires a non-linear power electronic device. Therefore, the power electronic device must be properly controlled to mitigate the impact of the unwanted power quality and to achieve efficient operation of the grid-connected PV system. A varying irradiance (Fig. 9) at 25 °C constant temperature was used to investigate the performance of the MRFO-based PI control strategy. The effectiveness of the MRFO algorithm was examined and justified by inserting the achieved optimal PI gain parameters (Table 4) into the developed model and comparing the results with those of the GOA, WOA, SSA, ASO, and GWO algorithms. Fig. 11, 12, and 13 show the responses of the active power, reactive power, and DC bus voltage, respectively, under the changing irradiation. The results showed that the responses of the MRFO and the other algorithms, except for ASO, operated at their fixed rated value under the operating conditions.
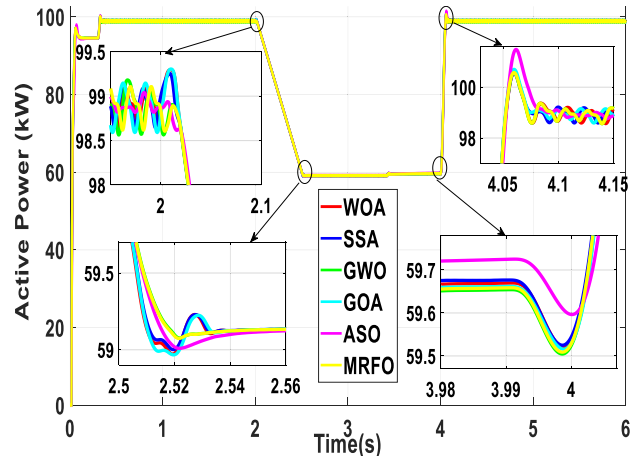

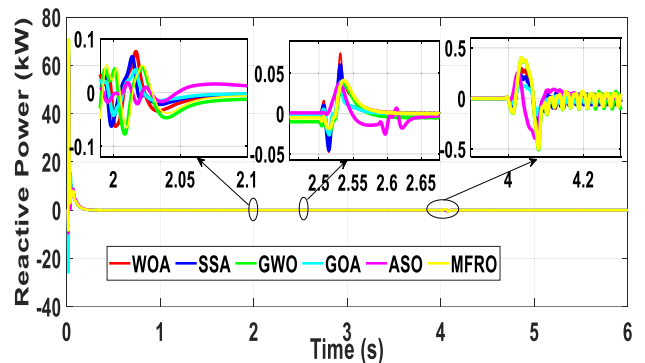**FIGURE 11.** Active power response to a change in irradiance.

FIGURE 12. Response of the reactive power to a change in irradiation.

Table 5 shows time-domain dynamic analysis of the system with ±5% and ±0.5% settling time for the active power and DC voltage respectively. The time-domain analysis is performed with MATLAB tool box for the first 1.5secs.

TABLE 4. Optimal PI parameters.

Algorithm	K$_{PDC}$	K$_{IDC}$	K$_{PI}$	K$_{II}$	K$_{PQ}$	K$_{IQ}$
GOA	0.081530072	6.549069514	0.005131172	0	0.002463605	0.321641966
GWO	0.1	7.193894945	0.00402648	0.000821042	0.0007554	0.186179081
WOA	0.1	7.097928537	0.004259032	0.007964969	0.00116634	0.209098212
ASO	0.1	3.583756045	0.004969222	0.084078725	0.002043977	0.365775977
SSA	0.1	7.789373007	0.004328082	0	0.001248091	0.280584647
MRFO	0.099999765	7.218847351	0.004030569	2.0752E-07	0.000761936	0.187330785

TABLE 5. Step-response analysis of the six algorithms.

Algorithm	DC-Voltage (pu)				Active Power(pu)			
	V_{peak}	$V_{steady\ state}$	$M_P(\%)$	t_{sec}	$Peak_{power}$	$P_{steady\ state}$	$M_p(\%)$	t_{sec}
MRFO	1.107264	1	10.7264	0.0709	1.011162	0.9909	1.1162	0.0507
GWO	1.107141	1	10.7141	0.0711	1.011163	1.000303	1.1163	0.0507
WOA	1.110059	1	11.0059	0.071	1.011213	1.000404	1.1213	0.0508
ASO	1.114062	1	11.4062	0.1098	1.010348	0.997071	1.0348	0.0512
SSA	1.120276	1	12.0276	0.0673	1.011279	1.000909	1.1278	0.0506
GOA	1.134898	1	13.4898	0.067	1.011663	1.000101	1.1663	0.0516
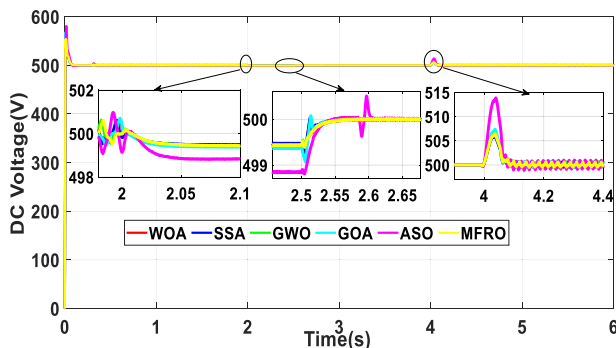
FIGURE 13. Response of the DC bus voltage to a change in irradiation.

The MRFO controller performance showed the best fitness solution with the best convergence rate compared with GOA, WOA, SSA, ASO, and GWO. The steady state operation of the system as demonstrated by time-domain analysis also reinforce robustness of the algorithm. The controller response was studied under constant and irradiance variation. The results demonstrated the capability of the proposed MRFO controller to solve the problems of non-linear system under uncertain conditions.

The reference voltage (1pu) is attained within a short time interval with minimal overshoot. More so, both the overshoot (M_p) and settling time for the active power are considerably low. These results demonstrate the ability of the MRFO controller to maintain stability within short time interval.

VI. CONCLUSION

This study demonstrated a new application of an MRFO-based PI controller with the determination to improve performance of the grid-connected PV system. The objective function and minimization of the fitness function were achieved by utilizing the ISE. Accordingly, MRFO-based PI-based controllers were used to enhance the operation of non-linear power electronic devices for an effective integration of the PV in the grid to achieve smooth power quality.

REFERENCES

[1] J. Mayer, D. Fuerstenwerth, S. Philipps, N. Saad Hussein, T. Schlegl, and C. Senkpiel, "Current and future cost of photovoltaics," Agora Energiewende, Berlin, Germany, Tech. Rep. 059/01-S-2015, 2015.

[2] A. Jäger-Waldau, *PV Status Report 2019*. Luxembourg, U.K.: Publications Office of the European Union, 2019.

[3] F.-J. Lin, K.-C. Lu, T.-H. Ke, B.-H. Yang, and Y.-R. Chang, "Reactive power control of three-phase grid-connected PV system during grid faults using Takagi–Sugeno–Kang probabilistic fuzzy neural network control," *IEEE Trans. Ind. Electron.*, vol. 62, no. 9, pp. 5516–5528, Sep. 2015, doi: 10.1109/TIE.2015.2407851.

[4] N. R. Merritt, C. Chakraborty, and P. Bajpai, "New voltage control strategies for VSC-based DG units in an unbalanced microgrid," *IEEE Trans. Sustain. Energy*, vol. 8, no. 3, pp. 1127–1139, Jul. 2017, doi: 10.1109/TSTE.2017.2657660.

[5] Y. Bak, J.-S. Lee, and K.-B. Lee, "Low-voltage ride-through control strategy for a grid-connected energy storage system," *Appl. Sci.*, vol. 8, no. 1, p. 57, Jan. 2018.

[6] X. Wang, Z. Yang, B. Fan, and W. Xu, "Control strategy of three-phase photovoltaic inverter under low-voltage ride-through condition," *Math. Problems Eng.*, vol. 2015, Dec. 2015, Art. no. 790584, doi: 10.1155/2015/790584.

[7] G. T. R. Gagnon, C. Larose, J. Brochu, G. Sybille, and M. Fecteau, "Large-scale real-time simulation of wind power plants into Hydro-Québec power system," in *Proc. 9th Int. Workshop Large-Scale Integr. Wind Power Syst. Well Transmiss. Netw. Offshore Wind Power Plants*, 2010, pp. 1–8.

[8] M. S. El Moursi, J. L. Kirtley, and W. Xiao, "Fault ride through capability for grid interfacing large scale PV power plants," *IET Gener., Transmiss. Distrib.*, vol. 7, no. 9, pp. 1027–1036, Sep. 2013, doi: 10.1049/iet-gtd.2013.0154.

[9] M. Russo and G. Fusco, "Robust decentralized PI controllers design for voltage regulation in distribution networks with DG," *Electr. Power Syst. Res.*, vol. 172, pp. 129–139, Jul. 2019, doi: 10.1016/j.epsr.2019.01.039.

[10] J. H. Holland, *Adaptation in Natural and Artificial Systems: An Introductory Analysis With Applications to Biology, Control, and Artificial Intelligence*. Ann Arbor, MI, USA: Univ. Michigan Press, 1975.

[11] S. Saremi, S. Mirjalili, and A. Lewis, "Grasshopper optimisation algorithm: Theory and application," *Adv. Eng. Softw.*, vol. 105, pp. 30–47, Mar. 2017, doi: 10.1016/j.advengsoft.2017.01.004.

[12] Z. Woo Geem, J. Hoon Kim, and G. V. Loganathan, "A new heuristic optimization algorithm: Harmony search," *SIMULATION*, vol. 76, no. 2, pp. 60–68, Feb. 2001, doi: 10.1177/003754970107600201.

[13] A. H. Gandomi, X.-S. Yang, and A. H. Alavi, "Cuckoo search algorithm: A Metaheuristic approach to solve structural optimization problems," *Eng. Comput.*, vol. 29, no. 1, pp. 17–35, Jan. 2013, doi: 10.1007/s00366-011-0241-y.

[14] W.-T. Pan, "A new fruit fly optimization algorithm: Taking the financial distress model as an example," *Knowl.-Based Syst.*, vol. 26, pp. 69–74, Feb. 2012, doi: 10.1016/j.knosys.2011.07.001.

[15] H. Eskandar, A. Sadollah, A. Bahreininejad, and M. Hamdi, "Water cycle algorithm–A novel metaheuristic optimization method for solving constrained engineering optimization problems," *Comput. Struct.*, vols. 110–111, pp. 151–166, Nov. 2012, doi: 10.1016/j.compstruc.2012.07.010.

[16] E. Rashedi, H. Nezamabadi-pour, and S. Saryazdi, "GSA: A gravitational search algorithm," *Inf. Sci.*, vol. 179, no. 13, pp. 2232–2248, Jun. 2009, doi: 10.1016/j.ins.2009.03.004.

[17] S. Mirjalili, S. M. Mirjalili, and A. Lewis, "Grey wolf optimizer," *Adv. Eng. Softw.*, vol. 69, pp. 46–61, Mar. 2014, doi: 10.1016/j.advengsoft.2013.12.007.

[18] S. Mirjalili, A. H. Gandomi, S. Z. Mirjalili, S. Saremi, H. Faris, and S. M. Mirjalili, "Salp swarm algorithm: A bio-inspired optimizer for engineering design problems," *Adv. Eng. Softw.*, vol. 114, pp. 163–191, Dec. 2017, doi: 10.1016/j.advengsoft.2017.07.002.

[19] W. Zhao, L. Wang, and Z. Zhang, "Atom search optimization and its application to solve a hydrogeologic parameter estimation problem," *Knowl.-Based Syst.*, vol. 163, pp. 283–304, Jan. 2019, doi: 10.1016/j.knosys.2018.08.030.

[20] S. Mirjalili and A. Lewis, "The whale optimization algorithm," *Adv. Eng. Softw.*, vol. 95, pp. 51–67, May 2016, doi: 10.1016/j.advengsoft.2016.01.008.

[21] R. Abdelrassoul, Y. Ali, and M. S. Zaghloul, "Genetic algorithm-optimized PID controller for better performance of PV system," in *Proc. World Symp. Comput. Appl. Res. (WSCAR)*, Mar. 2016, pp. 18–22.

[22] T. A. Jumani, M. W. Mustafa, M. M. Rasid, N. H. Mirjat, Z. H. Leghari, and M. S. Saeed, "Optimal voltage and frequency control of an islanded microgrid using grasshopper optimization algorithm," *Energies*, vol. 11, no. 11, p. 3191, Nov. 2018, doi: 10.3390/en11113191.

[23] M. N. Ambia, H. M. Hasanien, A. Al-Durra, and S. M. Muyeen, "Harmony search algorithm-based controller parameters optimization for a distributed-generation system," *IEEE Trans. Power Del.*, vol. 30, no. 1, pp. 246–255, Feb. 2015, doi: 10.1109/TPWRD.2014.2358940.

[24] R. N. Kalaam, S. M. Muyeen, A. Al-Durra, H. M. Hasanien, and K. Al-Wahedi, "Optimisation of controller parameters for grid-tied photovoltaic system at faulty network using artificial neural network-based cuckoo search algorithm," *IET Renew. Power Gener.*, vol. 11, no. 12, pp. 1517–1526, Oct. 2017.

[25] X. Zhang, G. Chen, and S. Jia, "Parameters optimization of PID controller based on improved fruit fly optimization algorithm," in *Proc. Int. Conf. Swarm Intell.*, 2018, pp. 421–431.

[26] H. M. Hasanien and M. Matar, "Water cycle algorithm-based optimal control strategy for efficient operation of an autonomous microgrid," *IET Gener., Transmiss. Distrib.*, vol. 12, no. 21, pp. 5739–5746, Nov. 2018, doi: 10.1049/iet-gtd.2018.5715.

[27] M. A. Attia, "Optimized controllers for enhancing dynamic performance of PV interface system," *J. Electr. Syst. Inf. Technol.*, vol. 5, no. 1, pp. 1–10, May 2018, doi: 10.1016/j.jesit.2018.01.003.

[28] H. Y. Mahmoud, H. M. Hasanien, A. H. Besheer, and A. Y. Abdelaziz, "Grey wolf algorithm as a solution for cascading control problem in converter based HVDC energy transmission system," in *Proc. 21st Int. Middle East Power Syst. Conf. (MEPCON)*, Dec. 2019, pp. 89–96.

[29] T. A. Jumani, M. W. Mustafa, M. M. Rasid, and Z. A. Memon, "Dynamic response enhancement of grid-tied ac microgrid using salp swarm optimization algorithm," *Int. Trans. Elect. Energy Syst.*, vol. 30, no. 5, 2020, Art. no. e12321, doi: 10.1002/2050-7038.12321.

[30] D. Allam, H. Mohamed, M. Al-Gabalawy, and M. B. Eteiba, "Optimization of voltage source inverter's controllers using salp swarm algorithm in grid connected photovoltaic system," in *Proc. 21st Int. Middle East Power Syst. Conf. (MEPCON)*, Dec. 2019, pp. 958–963.

[31] B. Hekimoglu, "Optimal tuning of fractional order PID controller for DC motor speed control via chaotic atom search optimization algorithm," *IEEE Access*, vol. 7, pp. 38100–38114, 2019.

[32] H. M. Hasanien, "Performance improvement of photovoltaic power systems using an optimal control strategy based on whale optimization algorithm," *Electric Power Syst. Res.*, vol. 157, pp. 168–176, Apr. 2018, doi: 10.1016/j.epsr.2017.12.019.

[33] W. Zhao, Z. Zhang, and L. Wang, "Manta ray foraging optimization: An effective bio-inspired optimizer for engineering applications," *Eng. Appl. Artif. Intell.*, vol. 87, Jan. 2020, Art. no. 103300, doi: 10.1016/j.engappai.2019.103300.

[34] H. Bellia, R. Youcef, and M. Fatima, "A detailed modeling of photovoltaic module using MATLAB," *NRIAG J. Astron. Geophys.*, vol. 3, no. 1, pp. 53–61, Jun. 2014, doi: 10.1016/j.nrjag.2014.04.001.

[35] A. Al-Shamma'a, A. Noman, K. Addoweesh, A. Alabduljabbar, and A. Alolah, "Analytical approach to circulating current mitigation in hexagram converter-based grid-connected photovoltaic systems using multi-winding coupled inductors," *Int. J. Photoenergy*, vol. 2018, May 2018, Art. no. 9164528, doi: 10.1155/2018/9164528.

[36] E. Koutroulis, K. Kalaitzakis, and N. C. Voulgaris, "Development of a microcontroller-based, photovoltaic maximum power point tracking control system," *IEEE Trans. Power Electron.*, vol. 16, no. 1, pp. 46–54, Jan. 2001, doi: 10.1109/63.903988.

[37] D. W. Hart, *Power Electronics*. New York, NY, USA: McGraw-Hill, 2011.

[38] M. Ahanch, M. S. Asasi, and M. S. Amiri, "A grasshopper optimization algorithm to solve optimal distribution system reconfiguration and distributed generation placement problem," in *Proc. IEEE 4th Int. Conf. Knowl.-Based Eng. Innov. (KBEI)*, Dec. 2017, pp. 0659–0666.

[39] A.-M.-M. Abdel-Rahim, S. A. Shaaban, and I. J. Raglend, "Optimal power flow using atom search optimization," in *Proc. Innov. Power Adv. Comput. Technol. (i-PACT)*, vol. 1, Mar. 2019, pp. 1–4.

FAHD A. ALTURKI received the B.S. degree in electrical engineering from King Saud University, Riyadh, Saudi Arabia, in 1986, the M.S. degree in control systems from Imperial College, London, U.K., in 1988, and the Ph.D. degree in control engineering from Sheffield University, Sheffield, U.K., in 1993. He was the Dean of the College of Engineering from 2008 to 2012. He has been the General Supervisor of King Saud University Colleges, Almuzahimiah Branch, since April 2013. He is currently an Associate Professor of Electrical Engineering with King Saud University. His main research interests include intelligent systems, signal processing, and nonlinear control.

HAMMED O. OMOTOSO received the bachelor's degree from the Ladoke Akintola University of Technology, Nigeria, in 2012, and the M.S. degree in electrical engineering from King Saud University, Riyadh, Saudi Arabia, in 2020.

He has worked as an Electrical Engineer with ADVAD Limited, Nigeria. He is currently working as a Researcher with the Department of Electrical Engineering, King Saud University. His research interests include smart grid, renewable energy resources, power electronics, and energy management.

ABDULLRAHMAN A. AL-SHAMMA'A was born in Sana'a, Yemen, in 1984. He received the bachelor's degree in electrical engineering-electrical power and machines from Sana'a University, Sana'a, in 2008, and the M.Sc. and Ph.D. degrees in electrical engineering from King Saud University, Riyadh, Saudi Arabia, in 2013 and 2019, respectively. In 2019, he joined King Saud University, where he is currently an Adjunct Assistance Professor with the Department of Electrical Engineering. His research interests include the design, controlling, and optimization of renewable energy systems, as well as multilevel power electronics converters for micro-grids and electric drive applications. In the field of multilevel converters, he received two patents for simple and efficient power converters, including applications to grid-connected photovoltaic plants. Also, he published many research articles in refereed journals in addition to many international conference papers.

His current research interests include renewable energy systems (wind and solar photovoltaic), distributed generation, power quality, power electronics applications, and smart control technologies (artificial intelligence and meta-heuristic optimization techniques). He published till now 27 articles in a highly reputable international journals, book chapters, and international conferences papers. Also, he is a reviewer of many reputed international journals. He worked in many technical projects and researches related to electrical power quality and renewable energy applications. Award-winning of Excellence in Scientific Research, College of Engineering, King Saud University, in 2013.

HASSAN M. H. FARH was born in Egypt, in January 1984. He received the B.Sc. degree (Hons.) from Zagazig University, Egypt, in 2006, and the M.Sc. degree from King Saud University, Saudi Arabia, in 2013, the first Ph.D. degree in electrical engineering and electrical power (photovoltaic energy systems) from Universiti Teknologi Malaysia (UTM), Malaysia, in 2019, and the second Ph.D. degree in electrical engineering and electrical power (renewable distributed generation) from King Saud University, in 2020. Over the past 12 years, he had the opportunity to teach a variety of electrical courses in the undergraduate program. He is currently working as a Researcher with the Electrical Engineering Department, College of Engineering, King Saud University.

KHALIL ALSHARABI was born in Taiz, Yemen, in 1983. He received the B.S. degree in communication and computer engineering from Taiz University, Yemen, in 2008, and the M.S. degree in electrical engineering and control systems engineering from King Saud University, Saudi Arabia, in 2017. He is currently pursuing the Ph.D. degree with the Electrical Engineering Department, King Saud University. His research interests include brain–computer interfaces, EEG signal processing, bioengineering systems, control systems engineering, and artificial intelligence.

● ● ●